Extracting a model quark propagator's spectral density

Zehao Zhu,[1,*] Khépani Raya,[1,2,†] and Lei Chang[1,‡]

[1]*School of Physics, Nankai University, Tianjin 300071, China*

[2]*Instituto de Ciencias Nucleares, Universidad Nacional Autónoma de México, Apartado Postal 70-543, C.P. 04510, CDMX, México*

(Received 17 August 2020; accepted 21 January 2021; published 9 February 2021)

We propose a practical procedure to extrapolate the spacelike quark propagator onto the complex plane, which follows the Schlessinger point method and the spectral representation of the propagator. As a feasible example, we employ quark propagators for different flavors, obtained from the solutions of their corresponding Dyson-Schwinger equation (DSE), with different truncations. Thus, the analytical structure of the quark propagator is studied, capitalizing on the current-quark mass dependence of the observed features.

DOI: 10.1103/PhysRevD.103.034005

I. INTRODUCTION

The strong-interactions part of the Standard Model of particle physics, quantum chromodynamics (QCD), is characterized by two emergent phenomena: dynamical chiral symmetry breaking (DCSB) and confinement [1]. DCSB is responsible for the vast majority of the mass of the visible universe and has a crucial impact on the observed hadron spectrum and properties; for example, it explains both the large mass of the proton and the unnaturally light mass of the pion. Confinement entails that colored states, such as QCD's fundamental degrees of freedom (quarks and gluons), cannot appear in the spectrum. It also guarantees that condensates, typical order parameters of DCSB [2], are wholly contained within hadrons [3]. Thus, DCSB and confinement might be, in fact, intimately connected. Both phenomena can be potentially understood from QCD's 2-point functions, namely, propagators. Studying the analytical properties of the propagators could shed some light [4,5] on their confinement properties and the connection with DCSB. Dyson-Schwinger equations (DSEs) have been a cornerstone in handling such endeavors [6,7]. Thus, focusing on the matter sector, we obtain the quark propagator (in the spacelike axis) through its corresponding DSE [8–10]. Subsequently, the Schlessinger point method (SPM) [11,12] is employed to extrapolate the propagator into the complex plane, allowing us to study the corresponding spectral function and its analytic structure. The article is organized as follows: in Sec. II we write the DSE for the quark propagator, the truncation and model inputs. Section III describes the SPM and the analytic continuation procedure. It is worth mentioning that the algorithm is quite general and can be employed to study different inputs, such as lattice QCD propagators and other Green functions. Section IV shows the numerical results, and Sec. V summarizes the obtained conclusions.

II. GAP EQUATION

The DSE for the quark propagator, *gap equation*, is the starting point for analyses of DCSB and confinement in the continuum, as well as the fundamental ingredient for hadron physics studies based upon Bethe-Salpeter or Faddeev equations [13]. The gap equation, in Euclidean space, reads

$$\begin{aligned} S_f^{-1}(p) &= Z_2(i\gamma\cdot p + m_f^{\rm bm}) + \Sigma_f(p), \\ \Sigma_f(p) &= \frac{4}{3} Z_1 \int_{dq}^{\Lambda} g^2 D_{\mu\nu}(p-q)\gamma_\mu S_f(q)\Gamma_\nu^f(p,q), \end{aligned} \quad (1)$$

where $\int_{dq}^{\Lambda} = \int^{\Lambda} \frac{d^4q}{(2\pi)^4}$ stands for a Poincaré invariant regularized integration, with Λ regularization scale. The rest of the pieces are defined as usual: S_f is the f-flavor quark propagator, $D_{\mu\nu}$ is the gluon propagator and Γ_ν the fully dressed quark-gluon vertex (QGV); $Z_{1,2}$ are the quark-gluon vertex and quark wave function renormalization constants, respectively; g is the Lagrangian coupling constant and $m_f^{\rm bm}$ is the bare-quark mass. The latter is related with the renormalization point (ζ) dependent current-quark mass, m_f^ζ, via Slavnov-Taylor identities [14,15]. Each Green function involved obeys its own DSE, thus forming an infinite tower of coupled equations, which must be systematically truncated to extract the encoded physics. Regardless of the truncation, a general

*1710315@mail.nankai.edu.cn
†khepani@nankai.edu.cn
‡leichang@nankai.edu.cn

solution for the fully dressed quark propagator can be expressed as follows

$$S_f(p) = Z_f(p^2)(i\gamma\cdot p + M_f(p^2))^{-1}, \tag{2}$$

in analogy with its bare counterpart,

$$S_f^{(0)}(p) = (i\gamma\cdot p + m_f^{\rm bm})^{-1}.$$

Here $Z(p^2)$ and $M(p^2)$ are dressing functions; the latter, independent of ζ, is known as the mass function. In the Rainbow approximation [16], Eq. (1) is modified according to the replacement:

$$g^2 Z_1 D_{\mu\nu}(p-q)\Gamma_\nu^f(p,q) \to Z_2^2 \tilde{D}_{\mu\nu}^f(p-q)\gamma_\nu, \tag{3}$$

where $\tilde{D}_{\mu\nu}^f(k) \coloneqq T_{\mu\nu}(k)\mathcal{G}^f(k^2) = (\delta_{\mu\nu} - k_\mu k_\nu/k^2)\mathcal{G}^f(k^2)$ and $\mathcal{G}^f(k^2)$ is the effective coupling, expressed as [16,17]:

$$\mathcal{G}^f(s=k^2) = \mathcal{G}_{\rm IR}^f(s) + \mathcal{G}_{\rm UV}^f(s), \tag{4}$$

$$\mathcal{G}_{\rm IR}^f(s) = \frac{8\pi^2 D_f^2}{\omega_f^4} e^{-s/\omega_f^2}, \tag{5}$$

$$\mathcal{G}_{\rm UV}^f(s) = \frac{8\pi^2\gamma_m \mathcal{F}(s)}{\ln[\tau + (1+s/\Lambda_{\rm QCD})^2]}. \tag{6}$$

The term $\mathcal{G}_{\rm IR}^f(s)$ provides an infrared enhancement, which is controlled by the product $\omega_f D_f^2$. Conversely, $\mathcal{G}_{\rm UV}^f(s)$ is set to reproduce the one-loop renormalization-group behavior of QCD in the gap equation. We have defined $s\mathcal{F}(s) = (1-\exp[-s/(4m_t^4)])$, $\gamma_m = 12/(33-2N_f)$, $\tau = e^{10}-1$, $m_t = 0.5$ GeV, $\Lambda_{\rm QCD} = 0.234$ GeV and $N_f = 5$. We solve Eq. (1) for different current-quark masses, whose specific values and interaction strength are given in Table I.

Key features of the gluon propagator, such as the infrared saturation and the connection with perturbation theory, are conveniently captured by the model defined in Eqs. (4)–(6). However, we shall also explore the renormalization-group-invariant (RGI) interaction described in [18], which is derived in connection with the process-independent strong running-coupling, obtained from lattice QCD's Green functions at the physical pion mass. Thus, those attributes of the QCD coupling are captured from a first principles approach. In this case, the leading-order QGV, γ_ν, turns out to be inadequate due to lack of tensor structures that enhance the contribution of the vertex to DCSB [19,20]. A minimal extension that makes the QGV compatible with [18] demands the inclusion of the anomalous chromomagnetic moment (ACM) term [21,22].

TABLE I. One-loop evolved current quark masses and gluon model parameters. Masses, ω_f and D_f are listed in GeV. The renormalization scale is set to $\zeta = 2$ GeV.

Flavor	m_f^ζ	ω_f	D_f^2
u/d	0.005	0.500	1.060
s	0.112	0.530	1.040
c	1.170	0.730	0.599
b	4.070	0.766	0.241

Thus, we explore a simple beyond-RL truncation (BYRL). In this case, the self-energy term in Eq. (1), $\Sigma(p)$, is recast as follows ($k = p - q$):

$$\Sigma(p) = Z_2 \frac{4}{3}\int_{dq}^{\Lambda} 4\pi \hat{d}(k) T_{\mu\nu}(k)\gamma_\mu S(q)\Gamma_\nu^{BY}(p,q), \tag{7}$$

$$\Gamma_\nu^{BY}(p,q) = Z_2\gamma_\nu + \eta\sigma_{\nu\alpha}k_\alpha \frac{B(p^2)-B(q^2)}{p^2-q^2}\mathcal{H}(k^2), \tag{8}$$

where $k = p - q$, $B(p^2) = M(p^2)/Z(p^2)$; $(s/m_0^2)\mathcal{H}(s) = (1 - e^{-s/m_0^2})$ is merely a profile function that controls the ultraviolet convergence and restricts the ACM effects to the infrared domain [21]; $m_0 = 2$ GeV and $\eta = 0.37$ are parameters; and, finally, $\hat{d}(k)$ is the effective interaction from Ref. [18]. For the time being, in the case of the proposed BY truncation, we shall restrict ourselves to the u/d quark.

III. ANALYTIC CONTINUATION

By solving the gap equation, it is *almost* straightforward to obtain the quark propagator in the $p^2 > 0$ axis. The extension to the complex p^2 plane can be numerically challenging since, among other issues, one might encounter singularities [23–28]. Thus, we follow an analytic continuation scheme, based upon the spectral representation [29–32] of the quark propagator and the SPM, to extrapolate our spacelike numerical solutions onto the complex plane.

For that purpose, it is convenient to reexpress the quark propagator, in Eq. (2), in terms of its vector (σ_V) and scalar (σ_S) dressing functions:

$$S_f(p) = -i\gamma\cdot p\sigma_V(p^2) + \sigma_S(p^2). \tag{9}$$

Both $\sigma_{V,S}(p^2)$ are obtained on a large, discrete set of points ($p_i^2 > 0$, $i = 1,\ldots,N$). Following the SPM, we employ a continued fraction representation such that

$$\begin{aligned}\sigma(p^2) &= \frac{\sigma(p_1^2)}{1^+}\frac{a_1(p^2-p_1^2)}{1^+}\cdots\frac{a_N(p^2-p_N^2)}{1}, \\ &= \sigma(p_1^2)\left[1 + \frac{a_1(p^2-p_1^2)}{1+\frac{a_2(p^2-p_2^2)}{1+\cdots}}\right]^{-1},\end{aligned} \tag{10}$$

provides a rational representation for these functions (the labels V, S are implicit). The coefficients a_i are recursively obtained, ensuring that $\forall\, p_i^2$, the interpolated value of $\sigma(p_i^2)$ exactly reproduces the numerically obtained one [11]. Therefore, as discussed in Ref. [31], the SPM gives almost exact reconstructions, of the continuous function, if the number of input points is adequate. Notice that Eq. (10) can be expressed as a rational fraction, $\sigma(p^2) = P(p^2)/Q(p^2)$, where P and Q are polynomials of p^2, whose degree is determined by the parity of N, the number of input points: if N is an odd number, both P and Q will have degree $(N-1)/2$; if N is even instead, then the order would be $N/2-1$ (for P) and $N/2$ (for Q). Therefore, the parity of N determines the asymptotic $p^2 \to \infty$ behavior (it is either a constant or exhibits a $1/p^2$ fall) and the number of poles, which are simply the roots of Q. As we shall discuss, most of these poles are neither physically nor numerically meaningful.

The obtained rational function will be employed to evaluate $\sigma(p^2)$ beyond the original input domain. Thus we allow the spacelike p^2 to take complex values. An important feature of the SPM is its capability to identify singularities and branch points [33]. For example, a series of poles along a line in the complex plane, typically indicates the presence of a branch cut [34]. However, it is seen that if p^2 remains real and positive in the training set, the SPM most likely will not introduce or detect any singular structure besides scattered poles. This is due to the simple shapes that $\sigma_{V,S}$ take on the spacelike axis: finite, continuous and monotonically decreasing functions. Thus, it is found advantageous to deal with a $\sqrt{p^2}$ grid instead [34]. The training set is plainly mapped as

$$\{p_i^2, \sigma(p_i^2)\} \to \left\{\sqrt{p_i^2}, \sigma(p_i^2)\right\}, \tag{11}$$

such that SPM is performed on the set $\{\sqrt{p_i^2}, \sigma(p_i^2)\}$ and a rational representation of the quark propagator is then obtained. Clearly, the mapping in Eq. (11) introduces branch cuts on the positive and negative imaginary axes. On the p^2 plane, this corresponds to a branch cut along the negative real axis. Besides, other singular structures, in the form of complex conjugate poles (CCP), could also appear dispersed on the complex plane [6,23]. The closed contours, which leave all the poles and branch cuts outside, are sketched in Fig. 1. One can see the connection between the $\sqrt{p^2}$ and p^2 planes and their corresponding, equivalent, integration contours.

At this point, one can appeal to complex analysis theorems to represent $\sigma(p^2)$ in a convenient manner. An arbitrary point inside the chosen contour can be written as a Cauchy integral. Moreover, from the residue theorem [35,36], the quark propagator can be usefully reexpressed as follows:

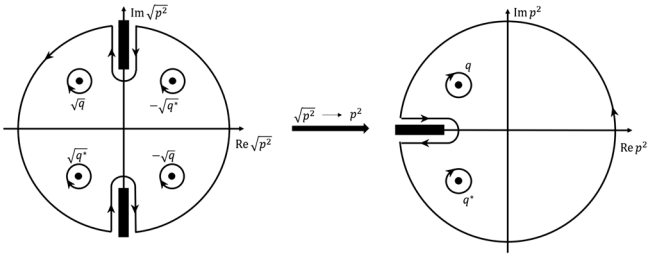

FIG. 1. Connection between the closed contours, corresponding to the $\sqrt{p}$ and p^2 planes. The contours keep all the poles outside and have a infinitesimal distance ϵ away from the branch cut(s). To calculate the Cauchy integral, the p^2 plane is simpler.

$$\sigma(p^2) - \frac{1}{\pi}\int_0^\infty \frac{\rho(\omega)}{p^2+\omega}d\omega = \sum_i \left(\frac{R_i}{p^2-q_i} + \frac{R_i^*}{p^2-q_i^*}\right),$$
$$\rho(\omega) = \mathrm{Im}[\sigma(-\omega - i\epsilon)], \tag{12}$$

where ϵ is a positive infinitesimal real number; R_i and q_i take complex values, which are, respectively, identified as the residues and poles. Notice that the above equation corresponds to the integration contour on the p^2 plane, Fig. 1, such that we obtain a more compact expression. For instance, a pair of CCPs on the p^2 plane corresponds to four poles on the $\sqrt{p^2}$ one. The integral part is a standard dispersion relation for the propagator, such that $\rho(\omega)$ defines its spectral function; the fraction part accounts for the possible presence of complex conjugate poles.

In principle, $\rho(\omega)$ can be computed straightforwardly from the SPM on the numerical data. However, there are many components that can impact the stability of the extrapolations. We have identified key factors which alter the outcome; in particular, the number of input points and their distribution play a crucial role. Thus, in order to get more accurate and stable results, we proceed as follows:

(i) Redistribute the big set of $N_p = m \cdot n$ points into n subsets of m points.
(ii) Randomly select one point from each subset, in order to form a new small set (of n points).
(iii) Implement SPM on the latter and produce a rational representation of $\sigma(p^2)$.
(iv) Repeat several times to obtain a mean value and error estimates.

This strategy makes it easy to control the number of points, while also covering most of the domain of the initial, much bigger, set. The SPM is performed several times, keeping the mean value as the final result and ensuring a small error is produced. Besides, the particular values of m and n are properly fixed by the requirement that the produced spectral functions are similar in shape and the location of the poles is stable. The latter is discussed below.

TABLE II. Chosen (m, n) values for each quark flavor; vector and scalar parts separately.

Flavor	Vector	Scalar
u/d	(42,24)	(16,60)
s	(10,24)	(16,64)
c	(28,36)	(32,8)
b	(6,38)	(42,24)

Another important point is the fact that $\rho(\omega)$ comes from the integral along a branch cut, corresponding to $p^2 < 0$. Although the SPM was performed on a $\sqrt{p^2}$ grid, we can establish the connection with the equivalent contour on the p^2 plane, as it is clear from Fig. 1. The presence of the branch cut serves a crucial purpose: it allows us to write the propagator as in Eq. (12), enabling access to its pole structure. An effective method to calculate the positions and residues of the poles has been already introduced in Refs. [37,38], but it is not practical enough to reconstruct the propagator.

On the other hand, the collection of complex poles which are obtained from the rational representation, Eq. (10), depends on the size of the input set, therefore yielding a number of *spurious* irrelevant poles. This is an undesirable aspect of relying completely on the SPM, which needs to be supplemented somehow. In Ref. [34], it was proposed to take into account only those poles

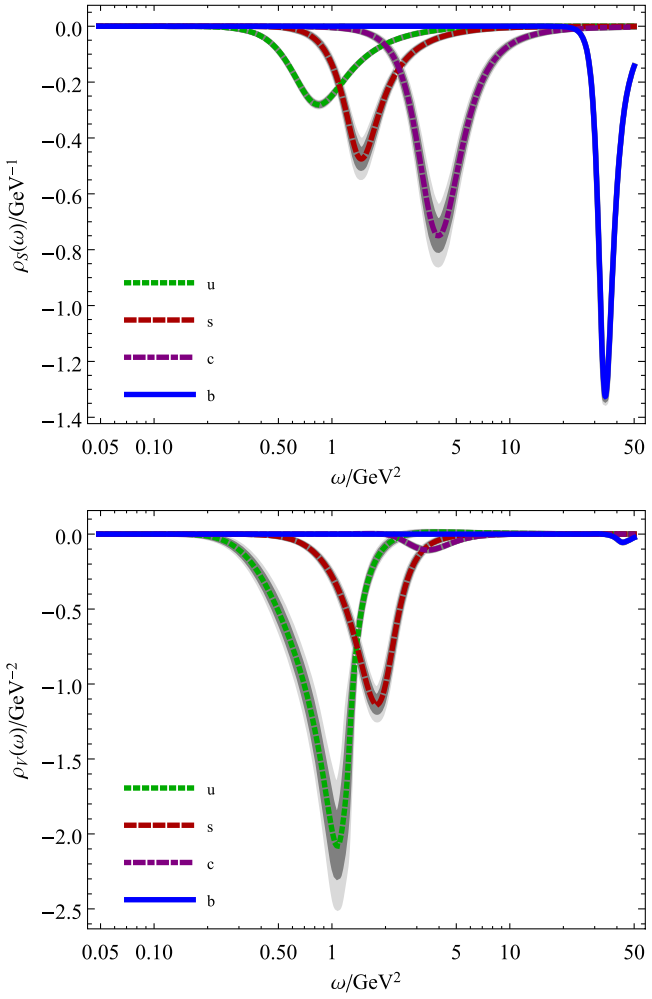

FIG. 2. Upper panel: spectral density associated with the scalar part of the propagator, $\sigma_s(p^2)$, in the RL truncation. Lower panel: the analogous for the vector part. The dark-gray and light-gray shaded areas represent the σ and 2σ confidence intervals, respectively. Consistently, the observed peaks are shifted towards $\omega \to \infty$ as the quark mass increases.

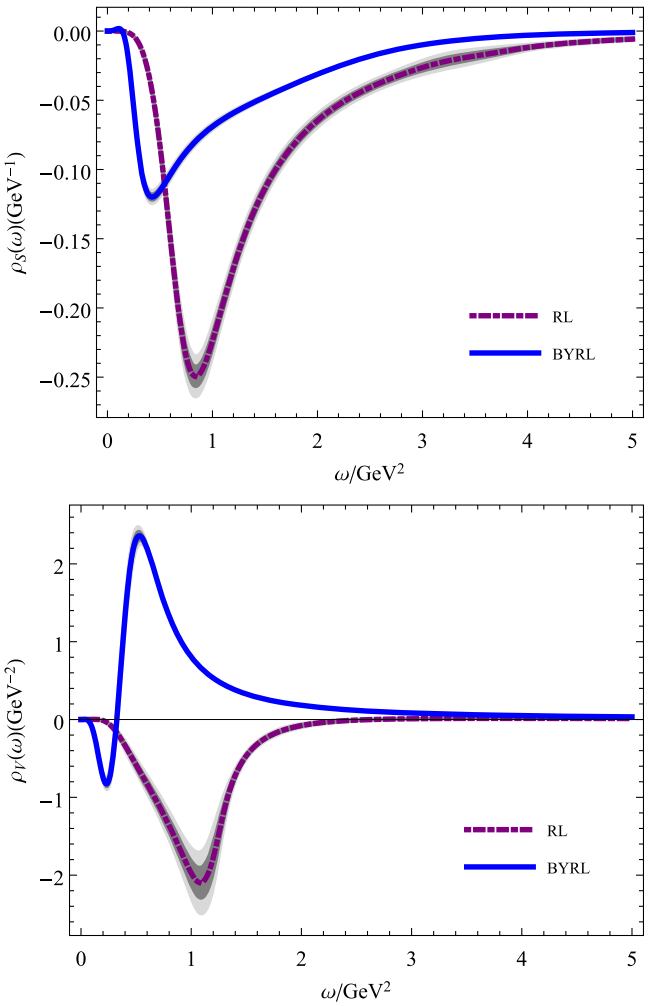

FIG. 3. Upper panel: comparison of RL and BYRL truncation results for the spectral density associated with the scalar part of the u-quark propagator, $\sigma_s(p^2)$. Lower panel: the analogous for the vector part. The dark-gray and light-gray shaded areas represent the σ and 2σ confidence intervals, respectively.

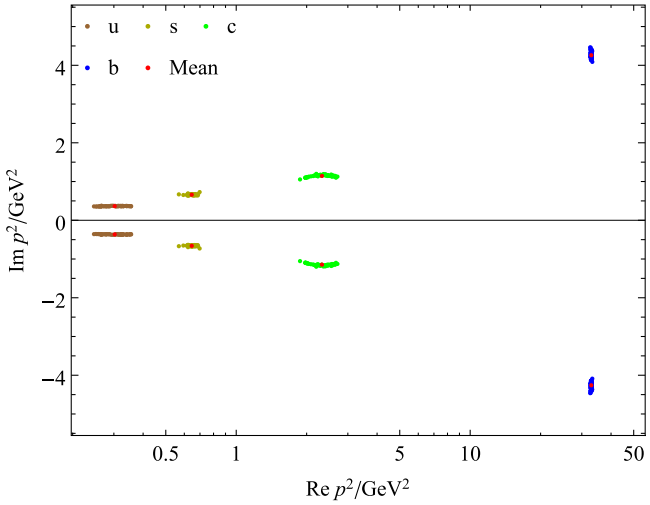

FIG. 4. Position of the poles (q) in the complex plane, with extrapolation uncertainty. From left to right: u, s, c and b quark propagators. The displayed results correspond to the RL truncation.

with residues above a certain threshold. This demands identifying all the poles produced from the rational interpoland (which might not be practical) and then use Eq. (12) to discriminate. We suggest an alternative which prevents us from performing such demanding task. With $\sigma(p^2)$ and $\rho(\omega)$ already at hand after performing the SPM several times, what is left to compute is the right-hand side of Eq. (12). This can be obtained by finding optimal values, of q_i and R_i, such that the left-hand side is reproduced with highest accuracy. In fact, we have seen that a single pair of CCPs is sufficient to accurately determine the quark propagator. This implies that Eq. (12) can be conveniently reduced to

$$\sigma(p^2) - \frac{1}{\pi}\int_0^\infty \frac{\rho(\omega)}{p^2+\omega}\,d\omega \simeq \left(\frac{R}{p^2-q} + \frac{R^*}{p^2-q^*}\right), \qquad (13)$$

TABLE III. Relevant poles (q) and residues (R) for different quark flavors. Top (bottom) panel corresponds to the RL (BYRL) truncation results. The mass units are expressed in appropriate powers of GeV.

Flavor	q	R [σ_v]	R [σ_s]
u/d	$-0.302 \pm 0.364i$	$0.586 \mp 0.542i$	$-0.013 \mp 0.480i$
s	$-0.646 \pm 0.660i$	$0.702 \mp 0.311i$	$0.060 \mp 0.719i$
c	$-2.325 \pm 1.145i$	$0.577 \mp 0.712i$	$1.098 \mp 0.157i$
b	$-32.942 \pm 4.260i$	$0.674 \pm 0.498i$	$5.110 \mp 3.287i$
u/d	$-0.175 \pm 0.210i$	$0.231 \mp 0.685i$	$0.001 \mp 0.390i$

such that, with $\rho(\omega)$ already calculated, q and R (poles and residues) can be straightforwardly identified following standard minimization procedures. As we shall see, the *leading* pair of CCPs (those closest to the origin on the complex plane), obtained from the rational representation of Eq. (10), coincide with q and q^*, ensuring the robustness of this approach.

IV. NUMERICAL RESULTS

From the solutions of the gap equation, Eq. (1), for different quark flavors (u/d, s, c, b), one gets the spacelike quark propagators. Following the SPM, the quark propagators extrapolated beyond their original domain. Then, the corresponding spectral functions; the

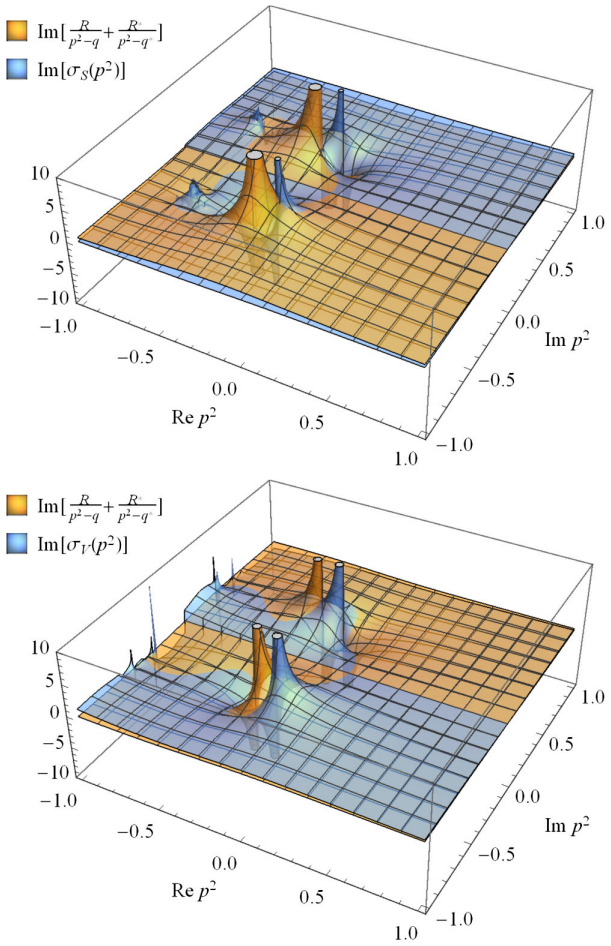

FIG. 5. Location of the poles of the quark propagator, according to the interpoland of Eq. (10) (blue, multiple pairs of CCPs) and the Cauchy integral, Eq. (13) (yellow, single pair of CCPs). The latter is assumed to be the relevant pair of CCPs. Upper panel: scalar part of the u-quark RL propagator. Lower panel: the analogous for the vector part.

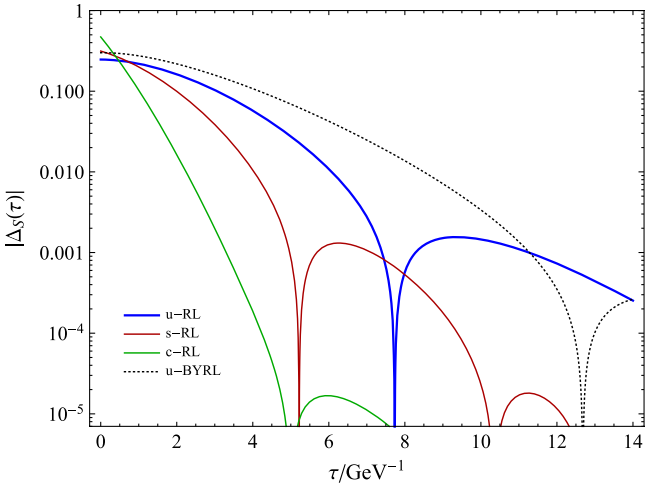

FIG. 6. Space averaged Schwinger functions of the scalar part of the RL propagators: u, s and c quarks. The presence of peaks, which move towards $\tau \to 0$ as the quark mass increases, reveals a change of sign in $\Delta_s(\tau)$. The first peak of the RL b-quark propagator lies around $\tau \sim 1$, but the Schwinger function becomes numerically unstable for larger values of τ.

relevant poles and their residues are identified following the algorithm described in the previous section. The SPM is performed 50 times for each quark flavor; the outputs are averaged to produce a final result and error estimates. The particular values of m and n, for each case, are specified in Table II.

The RL results for the spectral densities are displayed in Figs. 2 and 7; the latter shows the curves separately, for each quark flavor, and also includes the quark propagator dressing functions. As it is clear from these figures, the spectral densities are not positive definite. Moreover, both $\rho_s(w)$ and $\rho_v(w)$ consistently exhibit a peak (a minimum). Figure 3 compares the RL and BYRL results for the u/d quark. Notably, $\rho_s(w)$ follow the same pattern in both truncations and, although this does not happen for $\rho_v(w)$, it is important to highlight that the produced spectral densities are not positive definite in either case. Focusing on the RL case, it is seen that the position of the peak moves towards $\omega \to \infty$ as the current quark mass increases. For the scalar part, the absolute value of this minimum increases with the quark mass, while the opposite pattern is observed for the vector part. A natural kindred feature is also observed with the quark propagator dressing functions: at infrared momenta, the vector part of the u quark is much larger that its scalar counterpart; this is completely reversed for masses above $m_{\rm cr} \simeq m_c$. The position of the poles (with the associated uncertainty) as a function of the quark's mass is shown in Fig. 4. Their central values and the corresponding residues are captured in Table III. Evidently, the dominant poles move deeper into the complex plane as the current mass grows, i.e. it takes larger absolute values of both real and imaginary parts. This feature is consistent with realistic DSE studies [39,40]. It is worth mentioning that, although the rational interpoland of Eq. (10) introduces a collection of spurious meaningless poles, the *leading* CCPs almost coincide with the poles obtained from Eq. (13), as can be seen from Fig. 5. Similar outcomes are observed for the rest of the cases. This means, we do not require to compute all the poles obtained through Eq. (10) and identify the relevant ones somehow. Eq. (13) already provides such information and expedites the adequate identification.

The nonpositivity of the spectral functions [in particular $\rho_v(w)$] is often related to confinement [4,6], since it is a necessary (but not sufficient) condition. In this connection, we can also study the so-called spaced averaged (SA) Schwinger function [41], which, at $\vec{p} = 0$:

$$\Delta_{V,S}(\tau) := \int d^3x \int \frac{d^4p}{(2\pi)^4} e^{i(\tau p_4 + \vec{x}\cdot\vec{p})} \sigma_{V,S}(p_4^2),$$
$$= \frac{1}{\pi}\int_0^\infty dp_4 \cos(\tau p_4)\sigma_{V,S}(p_4^2). \tag{14}$$

The SA Schwinger function for a real, m massive, scalar particle will decay exponentially, $\Delta(\tau) \sim e^{-m\tau}$, since the propagator is simply $\sigma(p^2) = 1/(p^2 + m^2)$ and the mass shell can be reached in the real axis. On the other hand, if the quark propagator is described by a pair of CCPs instead, one should expect an oscillatory behavior, $\Delta(\tau) \sim e^{-a\tau}\cos(bt + \delta)$ (here, $m = a \pm ib$ are the CCP masses). In this case, the propagator could be associated with either a short-lived excitation that decays, or a confined, fundamental particle [6]. Figure 6 displays the SA Schwinger functions for the scalar parts of different quark flavors. The presence of the peaks in the logarithmic scale reveals a negative sign in the Schwinger function, thus another proof of violation of positivity. Naturally, the position of the peaks follow an opposite pattern, with respect to $\rho(\omega)$, i.e. peaks move towards $\tau \to 0$ with increasing current quark mass.

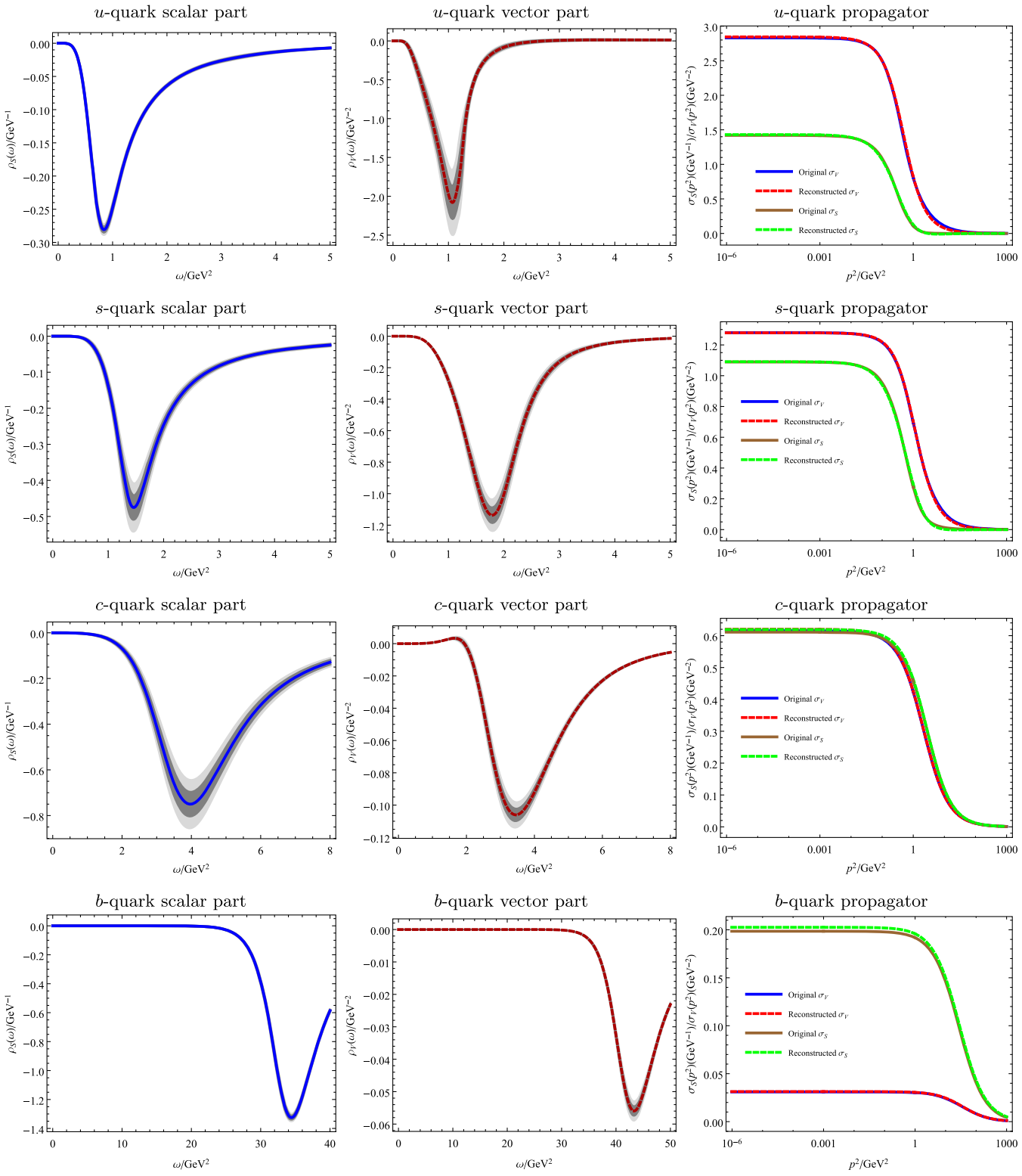

FIG. 7. The spectral densities and dressing functions for different quark masses, in the RL truncation. Left panel: scalar part, $\rho_s(\omega)$. Middle panel: vector part, $\rho_v(\omega)$. Right panel: quark propagator dressing functions: $\sigma_s(p^2)$, $\sigma_v(p^2)$. From *top* to *bottom*: u, s, c and b quarks. The depicted spectral functions are the mean result after 20 times SPM and analytic continuation. The dark-gray and light-gray bands represent σ and 2σ confidence intervals, respectively.

V. CONCLUSIONS AND SUMMARY

Starting with spacelike quark propagators, we described a viable procedure to get access to their complex structure. The DSE inputs have been employed merely as an illustration and the proposed method is quite general. This is based upon the SPM, which interpolates the spacelike quark propagator and extrapolates it into the complex plane. Then, a proper choice of integration contour allows us to rewrite the propagator in terms of a Cauchy integral, Eq. (12); thus defining the propagator's dressing functions in terms of spectral densities and granting us access to its pole structure. Remarkably, it is seen that a single pair of CCPs is sufficient to accurately represent the quark propagator, hence preventing us from the task of identifying and discriminating the *spurious* poles introduced by the rational interpoland, Eq. (10). Among other things, the representation of Eq. (13) could expedite the computation of the form factors, which typically require two pairs of CCPs [40,42–44] to give a precise result.

It is observed that the spectral densities are not positive definite and present peaks, which are shifted towards the ultraviolet region as the quark mass gets larger. Similarly, the position of the poles moves further into the complex plane with increasing current quark mass. The Schwinger functions exhibit the corresponding analogous features. Such consistency is encouraging. An immediate goal is to study whether or not the observed attributes are still valid for truncations beyond the RL approximation. In fact, we have proposed a simple RL extension that makes use of the novel process-independent strong running coupling [18] which, in contrast with the effective interaction that comes along with the RL truncation, is derived from a first principles approach to QCD's gauge sector. Our extension also includes the ACM term in the QGV, a crucial piece that is tightly connected with DCSB [20,21]. Limiting ourselves to the u/d quark, we have found that the produced spectral densities are not positive definite, as it also occurs with the RL truncation. This is a crucial characteristic that must prevail regardless of the current quark mass. The quantitative differences between the RL and BYRL result should be understood as follows: at the level of Green functions, the quantitative results shown should not be taken as the final answer; neither the RL or BYRL quark propagators correspond to the quark propagator of QCD in its full glory. Nevertheless, as has been known for several years, symmetry-preserving treatments of the RL truncation are adequate to describe a variety of hadron observables [1]. In that sense, our quantitative RL results should be useful and trusted.

Together with the practicality of our approach and the reduced error estimates, we believe that the algorithm discussed herein is also suitable to study other Green functions, since no assumptions on the form of $\sigma_{V,S}$ are made. Moreover, a domestic computer was sufficient to produce the results presented herein. Finally, it is worth recalling that the SPM has been proven useful in connecting Euclidean and Minkowskian quantities, a key goal in modern hadron physics, as well as a valuable extrapolation resource (see e.g. [45–48]). The present approach to obtain the analytical representation of the quark propagator would take potential roles in the calculation of the hadron spectrum, especially for the meson excited states.

ACKNOWLEDGMENTS

We are thankful to Daniele Binosi for sharing his code to implement the SPM, and appreciate the valuable comments provided by Alfredo Raya and José Rodríguez-Quintero. K. R. acknowledges support from CONACyT/México.

[1] C. D. Roberts, Empirical consequences of emergent mass, Symmetry **12**, 1468 (2020).
[2] A. Bashir, A. Raya, I. C. Cloet, and C. D. Roberts, Regarding confinement and dynamical chiral symmetry breaking in QED3, Phys. Rev. C **78**, 055201 (2008).
[3] S. J. Brodsky, C. D. Roberts, R. Shrock, and P. C. Tandy, Confinement contains condensates, Phys. Rev. C **85**, 065202 (2012).
[4] K. Osterwalder and R. Schrader, Axioms for Euclidean Green's functions. 2, Commun. Math. Phys. **42**, 281 (1975).
[5] T. Kugo and I. Ojima, Local covariant operator formalism of nonabelian gauge theories and quark confinement problem, Prog. Theor. Phys. Suppl. **66**, 1 (1979).
[6] R. Alkofer, W. Detmold, C. S. Fischer, and P. Maris, Analytic properties of the Landau gauge gluon and quark propagators, Phys. Rev. D **70**, 014014 (2004).
[7] P. Maris, A. Raya, C. D. Roberts, and S. M. Schmidt, Facets of confinement and dynamical chiral symmetry breaking, Eur. Phys. J. A **18**, 231 (2003).
[8] J. S. Schwinger, On the Green's functions of quantized fields. 1, Proc. Natl. Acad. Sci. U.S.A. **37**, 452 (1951).
[9] J. S. Schwinger, On the Green's functions of quantized fields. 2, Proc. Natl. Acad. Sci. U.S.A. **37**, 455 (1951).
[10] F. J. Dyson, The S matrix in quantum electrodynamics, Phys. Rev. **75**, 1736 (1949).
[11] L. Schlessinger, Use of analyticity in the calculation of nonrelativistic scattering amplitudes, Phys. Rev. **167**, 1411 (1968).
[12] L. Schlessinger and C. Schwartz, Analyticity as a Useful Computation Tool, Phys. Rev. Lett. **16**, 1173 (1966).
[13] C. D. Roberts and A. G. Williams, Dyson-Schwinger equations and their application to hadronic physics, Prog. Part. Nucl. Phys. **33**, 477 (1994).

[14] A. A. Slavnov, Teor. Mat. Fiz. **10**, 153 (1972) [Ward identities in gauge theories, Theor. Math. Phys. **10**, 99 (1972)].
[15] J. C. Taylor, Ward identities and charge renormalization of the Yang-Mills field, Nucl. Phys. **B33**, 436 (1971).
[16] S.-x. Qin, L. Chang, Yu.-x. Liu, C. D. Roberts, and D. J. Wilson, Interaction model for the gap equation, Phys. Rev. C **84**, 042202 (2011).
[17] M. Chen and L. Chang, A pattern for the flavor dependent quark-antiquark interaction, Chin. Phys. C **43**, 114103 (2019).
[18] Z.-F. Cui, J.-L. Zhang, D. Binosi, F. de Soto, C. Mezrag, J. Papavassiliou, C. D. Roberts, J. Rodríguez-Quintero, J. Segovia, and S. Zafeiropoulos, Effective charge from lattice QCD, Chin. Phys. C **44**, 083102 (2020).
[19] L. Albino, A. Bashir, L. X. Gutiérrez Guerrero, B. El Bennich, and E. Rojas, Transverse Takahashi identities and their implications for gauge independent dynamical Chiral symmetry breaking, Phys. Rev. D **100**, 054028 (2019).
[20] A. Bashir, R. Bermudez, L. Chang, and C. D. Roberts, Dynamical chiral symmetry breaking and the fermion–gauge-boson vertex, Phys. Rev. C **85**, 045205 (2012).
[21] L. Chang, Yu.-X. Liu, and C. D. Roberts, Dressed-Quark Anomalous Magnetic Moments, Phys. Rev. Lett. **106**, 072001 (2011).
[22] D. Binosi, L. Chang, J. Papavassiliou, S.-X. Qin, and C. D. Roberts, Natural constraints on the gluon-quark vertex, Phys. Rev. D **95**, 031501 (2017).
[23] M. Bhagwat, M. A. Pichowsky, and P. C. Tandy, Confinement phenomenology in the Bethe-Salpeter equation, Phys. Rev. D **67**, 054019 (2003).
[24] W. de Paula, T. Frederico, G. Salmè, M. Viviani, and R. Pimentel, Fermionic bound states in Minkowski-space: Light-cone singularities and structure, Eur. Phys. J. C **77**, 764 (2017).
[25] L. Chang, M. Chen, and Yu.-x. Liu, Excited B_c states via continuum QCD, Phys. Rev. D **102**, 074010 (2020).
[26] M. Chen, L. Chang, and Yu.-x. Liu, B_c Meson spectrum Via Dyson-Schwinger equation and Bethe-Salpeter equation approach, Phys. Rev. D **101**, 056002 (2020).
[27] F. F. Mojica, C. E. Vera, E. Rojas, and B. El-Bennich, Mass spectrum and decay constants of radially excited vector mesons, Phys. Rev. D **96**, 014012 (2017).
[28] T. Hilger, M. Gómez-Rocha, A. Krassnigg, and W. Lucha, Aspects of open-flavour mesons in a comprehensive DSBSE study, Eur. Phys. J. A **53**, 213 (2017).
[29] V. Sauli, Implications of analyticity to solution of Schwinger-Dyson equations in Minkowski space, Few Body Syst. **39**, 45 (2006).
[30] R.-A. Tripolt, J. Weyrich, L. von Smekal, and J. Wambach, Fermionic spectral functions with the functional renormalization group, Phys. Rev. D **98**, 094002 (2018).
[31] R.-A. Tripolt, P. Gubler, M. Ulybyshev, and L. Von Smekal, Numerical analytic continuation of Euclidean data, Comput. Phys. Commun. **237**, 129 (2019).
[32] Z. Wang and L. He, Fermion spectral function in hot strongly interacting matter from the functional renormalization group, Phys. Rev. D **98**, 094031 (2018).
[33] R.-A. Tripolt, I. Haritan, J. Wambach, and N. Moiseyev, Threshold energies and poles for hadron physical problems by a model-independent universal algorithm, Phys. Lett. B **774**, 411 (2017).
[34] D. Binosi and R.-A. Tripolt, Spectral functions of confined particles, Phys. Lett. B **801**, 135171 (2020).
[35] F. Siringo, Analytic structure of QCD propagators in Minkowski space, Phys. Rev. D **94**, 114036 (2016).
[36] F. Siringo, Dispersion relations for unphysical particles, EPJ Web Conf. **137**, 13017 (2017).
[37] A. Windisch, Analytic properties of the quark propagator from an effective infrared interaction model, Phys. Rev. C **95**, 045204 (2017).
[38] S. M. Dorkin, L. P. Kaptari, T. Hilger, and B. Kampfer, Analytical properties of the quark propagator from a truncated Dyson-Schwinger equation in complex Euclidean space, Phys. Rev. C **89**, 034005 (2014).
[39] L. Chang, I. C. Cloet, J. J. Cobos-Martinez, C. D. Roberts, S. M. Schmidt, and P. C. Tandy, Imaging Dynamical Chiral Symmetry Breaking: Pion Wave Function on the Light Front, Phys. Rev. Lett. **110**, 132001 (2013).
[40] K. Raya, M. Ding, A. Bashir, L. Chang, and C. D. Roberts, Partonic structure of neutral pseudoscalars via two photon transition form factors, Phys. Rev. D **95**, 074014 (2017).
[41] A. Bashir, A. Raya, and S. Sanchez-Madrigal, Chiral symmetry breaking and confinement beyond rainbow-ladder truncation, Phys. Rev. D **84**, 036013 (2011).
[42] L. Chang, I. C. Cloët, C. D. Roberts, S. M. Schmidt, and P. C. Tandy, Pion Electromagnetic form Factor at Spacelike Momenta, Phys. Rev. Lett. **111**, 141802 (2013).
[43] K. Raya, L. Chang, A. Bashir, J. J. Cobos-Martinez, L. X. Gutiérrez-Guerrero, C. D. Roberts, and P. C. Tandy, Structure of the neutral pion and its electromagnetic transition form factor, Phys. Rev. D **93**, 074017 (2016).
[44] M. Ding, K. Raya, A. Bashir, D. Binosi, L. Chang, M. Chen, and C. D. Roberts, $\gamma^*\gamma \to \eta, \eta'$ transition form factors, Phys. Rev. D **99**, 014014 (2019).
[45] M. Ding, K. Raya, D. Binosi, L. Chang, C. D. Roberts, and S. M. Schmidt, Symmetry, symmetry breaking, and pion parton distributions, Phys. Rev. D **101**, 054014 (2020).
[46] L. Liu, L. Chang, and Yu.-x. Liu, A bridge from Euclidean nonperturbative approach to Minkowskian distribution functions, arXiv:1912.09048.
[47] J. H. A. Nogueira, D. Colasante, V. Gherardi, T. Frederico, E. Pace, and G. Salmè, Solving the Bethe-Salpeter equation in Minkowski space for a fermion-scalar system, Phys. Rev. D **100**, 016021 (2019).
[48] Y.-Z. Xu, D. Binosi, Z.-F. Cui, B.-L. Li, C. D. Roberts, S.-S. Xu, and H. S. Zong, Elastic electromagnetic form factors of vector mesons, Phys. Rev. D **100**, 114038 (2019).